MXene

Subjects: Nanoscience & Nanotechnology

Contributor: Cheng-Feng Du

The MXenes are a kind of 2D metal carbide/nitride with an alternative atomic arrangement of Mn+1Xn (M = transition metals; X = C, N; n = 1, 2, 3, 4).

MXene | 2D materials | organic hybrids | energy storage

1. Structure and Surface Characters of MXenes

Take the $Ti_3C_2T_x$ MXene as an example. The Ti_3C_2 skeleton can be regarded as an extracted layer from *fcc* metal carbides lattice along (111) plane (Figure 1). Since the first discovery of $Ti_3C_2T_x$ MXene in 2011, more than 70 MXenes have been theoretically predicted or synthesized. As mentioned above, the synthesis of MXene follows a "top-down" protocol: selective etching of the A atoms from MAX phase ceramics. However, as the $M_{n+1}X_n$ layers and A atoms are alternatively arranged in MAX phase ceramics, the removal of A atoms will break M-A bonds, thus results in high-active M atoms at the surface. As first presented by Gogotsi et al., the surface terminal groups (T groups, e.g., –F, –O, or –OH) are necessary for stabilizing MXenes due to the high activity of these coordination unsaturated surface metal atoms [1]. Furthermore, owning to these surface terminal groups, the MXenes with typical inorganic carbide skeleton usually presents similar surface physicochemical properties (e.g., hydrophilicity and oxidizability) [2].

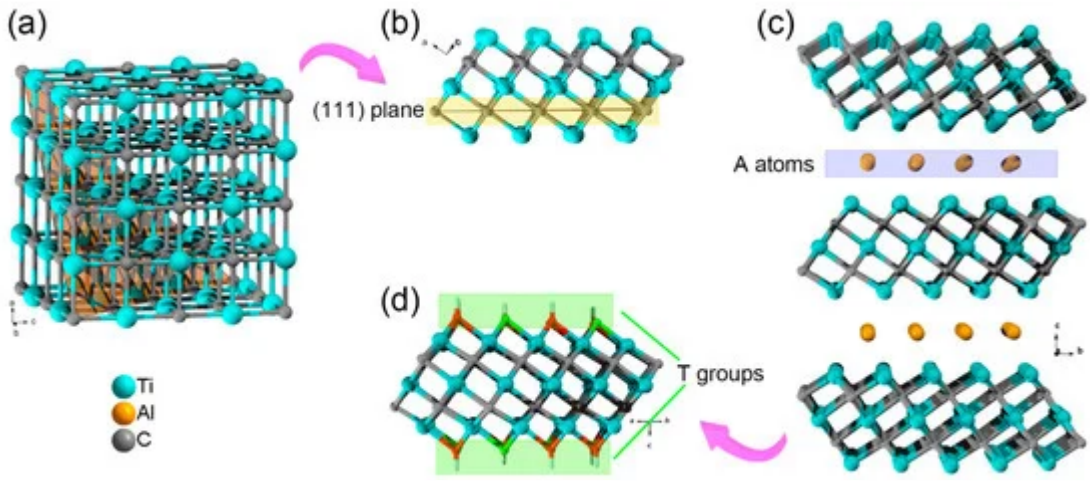

Figure 1. (**a**) A typical *fcc* lattice of TiC. (**b**) The extracted layer from *fcc* TiC lattice along (111) plane. (**c**) The side view of Ti_3AlC_2 lattice and (**d**) a monolayer of $Ti_3C_2T_x$ MXene.

Attributing to the surface T groups, the fresh MXene flakes are negatively charged and highly hydrophilic, which will form the colloidal dispersion by surface electrostatic repulsion. Based on the double electrical layer theory, it is easy to speculate that the dispersity of MXene flakes will change along with different solution conditions. Also depends on the average oxidation states of the M and X elements, the Zeta potential of MXenes is varied. In the past several years, the oxidation of MXenes in water also arouses wide concerns, which is found to be isogenesis with their hydrophilic. Still exampled by $Ti_3C_2T_x$ MXene, although TiO_2 species are detected when annealing the MXene under either vacuum, inert atmosphere (Ar, N_2), or oxidizing atmosphere (CO_2, air), the oxidation can be dramatically slowed down by decrease the environment temperature. However, in an aqueous suspension, nearly half of the flakes degrade in five days, even at room temperature [3][4]. The degradation behavior of MXenes in the aqueous suspension then can be ascribed to the water or the synergy of water and dissolved oxygen molecules. Interestingly, Kathleen et al. found that with oxygen solubility orders of magnitude higher than water, the organic solvent (N,N-dimethylformamide (DMF), 1-methyl-2-pyrrolidinone (NMP), propylene carbonate (PC), and ethanol) did not cause observable oxidation of MXenes [5]. Therefore, a deeper insight into the relationship between the surface T groups on $Ti_3C_2T_x$ MXene and their dispersion properties was presented, namely, the surface tension, polarity index, dielectric constant (ε), and cohesive energy density (δ). However, although some of the organic solvents were screened out to be a good medium for $Ti_3C_2T_x$ MXene dispersion, the dispersibility of $Ti_3C_2T_x$ MXene in nonpolar organic solvents is still an unsolved issue. What is more, the T groups usually have a random constituent and distribution, which makes the determination of surface properties more difficult.

Enlightened by traditional strategies towards surface compatibility regulation, the surface physicochemical properties of MXenes also can be dramatically altered by replacing the inorganic surface terminal groups with organic species. For example, di(hydrogenated tallow)benzyl methyl ammonium chloride (DHT)-treated $Ti_3C_2T_x$ MXene has shown a good dispersibility in nonpolar organic solvents [6]. More importantly, the study opens up a new way for MXene-polymer hybrids, which have good interfacial compatibility. In the following section, based on the interaction between organic species and MXenes, the synthesis and corresponding surface physicochemical properties of MXene-organic hybrids will be briefly discussed.

2. MXene-Organic Hybrids through Covalent Interaction

Benefiting from the surface atomic layers of early transition metals with empty *d* orbital, the MXenes skeleton usually presents a strong affinity to electron donors. When the organic molecules with electron-donating groups are introduced, the original T groups can be replaced. To date, numerous small organic molecules are found to be able to covalently connect on MXenes.

Silane ($RSiX_n$), one of the most commonly used organic coupling agents, has been widely applied for surface modification of inorganic materials. For silane, the R represents the functional group, such as an amino, alkane, aromatic group, epoxy group, and so on; X stands for hydrolysis group, containing Cl, OMe, OEt, etc. [7]. During the so-called “hydrolytic condensation” process (Figure 2a), X groups will first be hydrolyzed to form a siloxane (–SiOH) structure. Later, the siloxane goes through a dehydration condensation reaction to form oligomers. The –OH groups in oligomers will react with –OH groups on MXenes, forming an intermediate state. Finally, the Ti–O–Si

covalent bonds are formed by dehydration condensation [7][8]. Meanwhile, different properties inherited from *R* groups can be introduced into the inorganic phase. In 2018, Zhao et al. reported a trimethoxy (1H,1H,2H,2H-perfluorodecyl) silane (PFDTMS) modified $Ti_3C_2T_x$ MXene membrane prepared via a simple wet route [8], in which the water contact angle increased from 38.8° to 102.0° after PFDTMS grafting. Later, Sehyeong et al. have systematically studied the surface polarity regulation of $Ti_3C_2T_x$ MXene by silane with different R groups. After replacing the surface T groups of $Ti_3C_2T_x$ MXene with lipophilic octyltriethoxysilanes (OTS) [9], the OTS@MXene showed a water contact angle of 102.6° and exhibited excellent dispersion stability in non-polar hexane for more than four weeks. When methyltriethoxysilane (MTS), propyltriethoxyislane (PTS), and hexyltriethoxysilane (HTS) was selected, the surface hydrophobicity of these silane-MXene hybrids would decrease with shortening the alkyl chain. Beyond the randomly surface grafting, Zhang et al. designed a well-ordered vertically aligned Janus MXene-based aerogel, which has different wettability belong to two sides named VA-MXA [10]. After modifying the $Ti_3C_2T_x$ MXene by fluorinated alkyl silane under vacuum conditions, the water contact angle of the upper layer increased from 44.6° to 133.2°. Also, the excessive concentration of silane clogged the available surface and decreased the hydroxyls on the surface of $Ti_3C_2T_x$, which can bring novel surface physicochemical properties [7]. In Tran and his co-workers' work [11], the N,N-(diethylamino)dithiocarbamoyl-benzyl(trimethoxy) silane (SBDC) was used to functional Ti_2CT_x. Interestingly, the SBDC-MXene hybrid was applied as both substrate and iniferter, which allowed further polymerization of thermoresponsive polymer (poly(2-(dimethylamino)ethyl methacrylate (PDMAEMA)) on the surface of Ti_2CT_x. On the other hand, the silane molecules can not only change the surface hydrophilcity, but also alter the surface charged state (zeta potential) of MXenes. For instance, the aminosilane with positively charged amino group was demonstrated to have a critical role on the surface charge of aminosilane-$Ti_3C_2T_x$ hybrids [12][13]. As reported by Hossein et al. the [3-(2-aminoethylamino)propyl]-trimethoxy silane (AEAPTMS)-$Ti_3C_2T_x$ hybrids had a positive zeta potential of +62 mV at pH = 2.58, which is the highest zeta potential reported for MXenes to date. Similar to silane, the alkylphosphoric acid can also form covalent bonds with MXene through dehydration condensation reaction. Kim et al. demonstrated a simultaneous interfacial chemical grafting and phase transfer method for alkylphosphoric acid (C_nPA, n = 3, 6, 8, 10, 12) grafting on the $Ti_3C_2T_x$ flakes [14]. During the reaction, Ti–O–P bonds formed by interfacial nucleophilic addition and sequential condensation reaction between hydroxyl groups from $Ti_3C_2T_x$ and phosphate group from C_nPA. The pH and concentration of C_nPA are found to influence the interfacial chemical reaction and phase transfer. Whereas the dispersion stability of the $Ti_3C_2T_x$-C_nPA hybrids in nonpolar organic medium can be attributed to the steric stabilization and strong nonpolar interaction of long alkyl chains. Very recently, Sun et al. proposed new evidence on the existence of hydrogen bonds between $Ti_3C_2T_x$ nanosheets and C_8PA [15]. Therefore, it seems that the surface interaction between MXenes and coupling agents may be more complicated than we think.

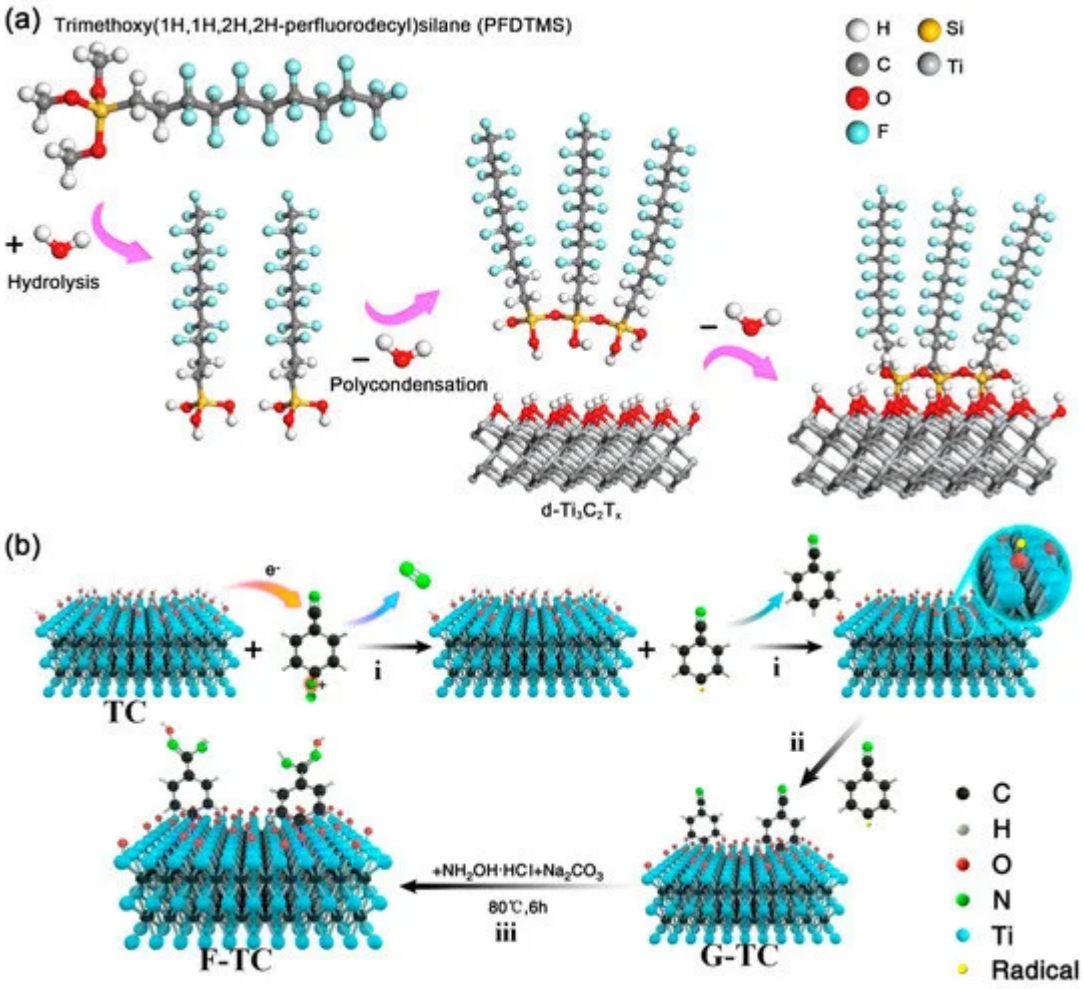

Figure 2. (**a**) Surface modification process of d-$Ti_3C_2T_x$ nanosheets by PFDTMS; Reproduced with permission [8]. Copyright 2018, Royal Society of Chemistry. (**b**) Proposed mechanism of amidoxime functionalization for MXene $Ti_3C_2T_x$; Reproduced with permission [16]. Copyright 2020, American Chemical Society.

Diazonium salt is another commonly used reagent to covalently connect organic functional groups on MXenes. In 2020, Zhang et al. first proposed a detailed reaction mechanism between aryl diazonium salts and $Ti_3C_2T_x$ MXene, in which the aromatic primary amine can undergo a diazotization reaction and the produced diazonium salts will covalently bond with MXenes. As shown in Figure 2b, the detailed reaction mechanism can be divided into three steps [17][16]: (1) an electron was transferred from $Ti_3C_2T_x$ MXene to aryl diazonium salt, which resulted in the cleavage of diazonium to nitrogen and aromatic free radical; (2) the aromatic free radical received an additional H atom from $Ti_3C_2T_x$ MXene, generating a Ti–O radical on the surface of MXene; (3) strong Ti–O–C covalent bonds formed between Ti–O radical and aromatic free radical. In fact, sulfanilic acid diazonium salts were introduced to get large-scale delaminated $Ti_3C_2T_x$ multilayers as early as 2016 [18][19][20]. Compared with the pristine $Ti_3C_2T_x$, the phenylsulfonic acid grafted $Ti_3C_2T_x$ MXene becomes amphiphilic material, which shows an increased solubility and excellent stability in water for more than one month. However, in consideration of the potential aromatic π interaction and the oxygen from the sulfonic group, the works did not give a detailed mechanism and solid evidence on the formation of MXene-aryl (Ti–O–C) linkages. Recently, Muhammad et al. compared the noncovalent and covalent interaction mechanism of 1-aminoanthraquinone (AQ) on $Ti_3C_2T_x$ MXene (denoted as

AQ@$Ti_3C_2T_x$ and AQ-$Ti_3C_2T_x$, respectively) [21]. It is found that after the diazonium reaction, the amino group disappeared, and the covalent bond formed between AQ and $Ti_3C_2T_x$. As observed, the covalently attached AQ on $Ti_3C_2T_x$ MXene offered better charge transportation, thus electrochemical performance. According to the abovementioned works, the diazonium reaction can be a useful way for the covalent connection of organic molecules onto the MXene nanosheets and further expands the applications of MXene-organic hybrids.

Taking advantage of the electrical conductivity and layered structure of MXenes, the MXene-polymer hybrids usually show improved properties when compared with the pure polymer, such as mechanical properties [22][23][24][25], flame retardancy [26][27], and responsiveness [11][28]. In early 2015, an MXene-organic hybrid with CO_2 and temperature dual-responsive property was reported by Chen et al. [28]. The hybrid consisted of V_2CT_x MXene and self-initiated photo grafting and photopolymerized (SIPGP) poly(2-(dimethylamino)ethyl methacrylate) (PDMAEMA) brushes. The hydroxyl groups on V_2CT_x MXene were acting as the photoactive sites, which allowed further growth of polymer brushes via SIPGP. When pre-modified MXene by SBDC [11], PDMAEMA brushes can also be connected onto the MXene surface. Zhang et al. [29] utilized in situ free radical polymerization to prepare $Ti_3C_2T_x$/polyacrylamide (PAA) hybrid with acrylamide monomer and potassium persulfate as redox initiator, in which the $Ti_3C_2T_x$ MXene was introduced as the crosslinker.

3. MXene-Organic Hybrids through Electrostatic Interaction

In addition to utilizing T groups of MXenes to covalently graft organic molecules by chemical reactions, the electrostatic interactions on negatively charged MXenes surface can also be utilized. Cui et al. synthesized the (3-aminopropyl) triethoxylsilane (APTES) grafted Si nanoparticles first [30], in which the covalently X groups on silane were consumed. However, by directly using the positively charged Y group (here, amino), the grafted Si nanoparticles were still self-assembled with $Ti_3C_2T_x$ through electrostatic interaction. Xu et al. reported microcontact printing to get ultrathin MXene micropatterns [31]. The MXene ink was applied to a polydimethylsiloxane (PDMS) film with patterns of alternating grooves. Subsequently, transfer printing it onto APTES-modified coverslips. In contrast, $Ti_3C_2T_x$ adsorbed onto coverslips by electrostatic interaction with amino groups.

As another kind of common-used organic molecules, alkylammonium salts including dodecyl trimethyl ammonium bromide (DTAB), tetradecyltrimethylammonium bromide (TTAB), cetyltrimethylammonium bromide (CTAB), stearyl trimethyl ammonium bromide (STAB), octadecyl trimethyl ammonium bromide (OTAB), dioctadecyl dimethyl ammonium chloride (DDAC), dihexadecyl dimethyl ammonium bromide (DDAB), and DHT are usually used to insert in MXene layers through electrostatic adsorption. After pillared by alkylammonium, the $Ti_3C_2T_x$ MXene presented a dramatic increase in interlayer spacing [32][33]. Obviously, the interlayer spacing increased along with the increasing length of alkyl chains [34]. Bian et al. proposed that the positively charged ammonium group might mainly be anchored on the surface –O groups from $Ti_3C_2T_x$ MXene [35], and the intercalation of alkylammonium can also affect the wettability of MXene (Figure 3a). Maybe because of the competitive adsorption of cations, the CTA cation pillared $Ti_3C_2T_x$ MXene can only form a stable oil-in-water emulsion in neutral or basic condition. While in acidic conditions, the MXene will aggregate at the oil/water interface. In a current study reported by Michael et

al., the DHT not only improved the organophilic nature of $Ti_3C_2T_x$, produced stable colloidal suspensions of $Ti_3C_2T_x$ in nonpolar solvents but also shielded the MXene flakes from oxidation in water [6].

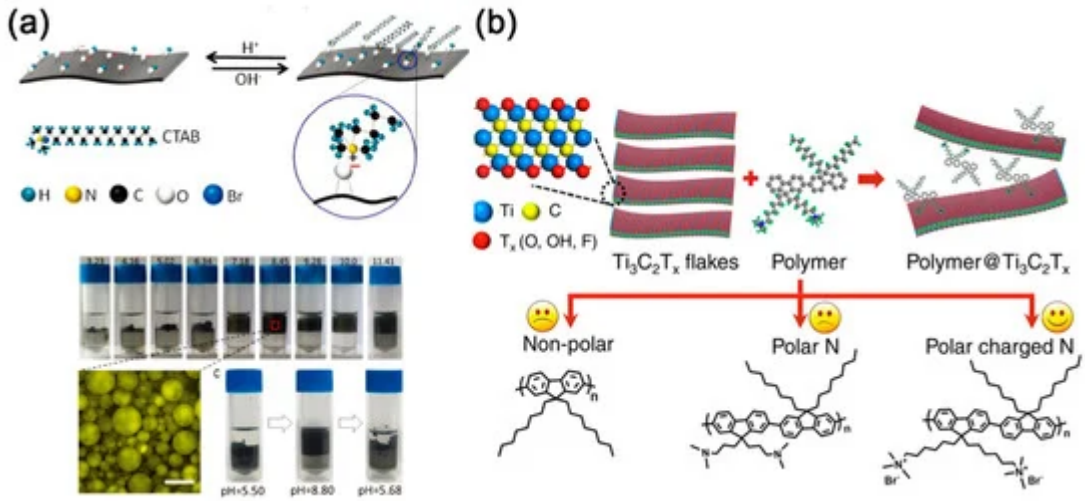

Figure 3. (**a**) Top: a possible scheme describing the interaction between cetyltrimethylammonium bromide (CTAB) and $Ti_3C_2T_x$ MXene. Bottom: the emulsion stability as a function of the pH of the aqueous phase at a fixed weight ratio of CTAB to MXene; reproduced with permission [35]. Copyright 2018, Royal Society of Chemistry. (**b**) Schematic illustration of the interaction of the polymer with $Ti_3C_2T_x$ layers (top) and the synthesized polymers with nonpolar, polar, and polar charged nitrogen lateral chain ends (bottom); Reproduced with permission [36]. Copyright 2017, American Chemical Society.

Amino acids are also studied as the organic part towards MXene-organic hybrids. Elumalai et al. proposed that the electrostatic interaction between –OH and –F groups on $Ti_3C_2T_x$ MXene and the zwitterion consisted of amino acid molecules might be the driving force for the spontaneous intercalation [37]. The MXene hybrids contained negatively charged glycine (Gly), phenylalanine (Phe), tryptophan (Trp), and histidine (His) can form stable suspensions in water due to the interparticle electrostatic repulsion. Whereas aromatic (Phe, Trp, His) intercalation may also produce rutile TiO_2@$Ti_3C_2T_x$ by sonication. On the contrary, combined with first principle calculations (DFT), recently, Chen et al. studied the interaction between Gly and double-layer structure $Ti_3C_2O_2$ [38]. From their analysis, the Ti and N atoms from $Ti_3C_2O_2$ and Gly, respectively, were likely to share electrons and lead to the formation of Ti–N bonding. Obviously, the ionizable organic molecules are another good choice for preparing MXene-organic hybrids with controllable properties. However, the unclear interaction mechanism makes it an urgent task to be solved.

Carey and his coworkers prepared the 12-aminolauric acid (ALA), or DHT-modified $Ti_3C_2T_x$ first (denoted as ALA-$Ti_3C_2T_x$ and DHT-$Ti_3C_2T_x$) [39][40]. After the modification, MXene changed from hydrophilic to organophilic, so the intercalation of the ε-caprolactam monomer and 6-aminocaproic acid catalyst was easier [39]. Additionally, uniform $Ti_3C_2T_x$ MXene/epoxy hybrids can be synthesized by ALA-$Ti_3C_2T_x$ and DHT-$Ti_3C_2T_x$. The authors proposed that ALA and DHT can speed up the curing reaction of epoxy in the interlayer space, which further enlarged the interlayer space of the MXene layers [61].

Similarly, the aniline monomers are believed to electrostatically adsorb on and between the multilayer MXene nanosheets [41]. Fu et al. reported a graphene-encapsulated Ti_2CT_x@polyaniline (PANI) hybrid named GMP for supercapacitors [42]. The adsorbed aniline monomers can be chemical oxidative polymerized with ammonium persulfate as the oxidant to form Ti_2CT_x@PANI hybrid (Figure 4). For graphene encapsulation, CTAB was utilized to lower the surface energy and change the zeta potential of Ti_2CT_x@PANI. Recently, there is also evidence that the surface functional groups on MXenes will facilitate nucleation during the PANI polymerization [43].

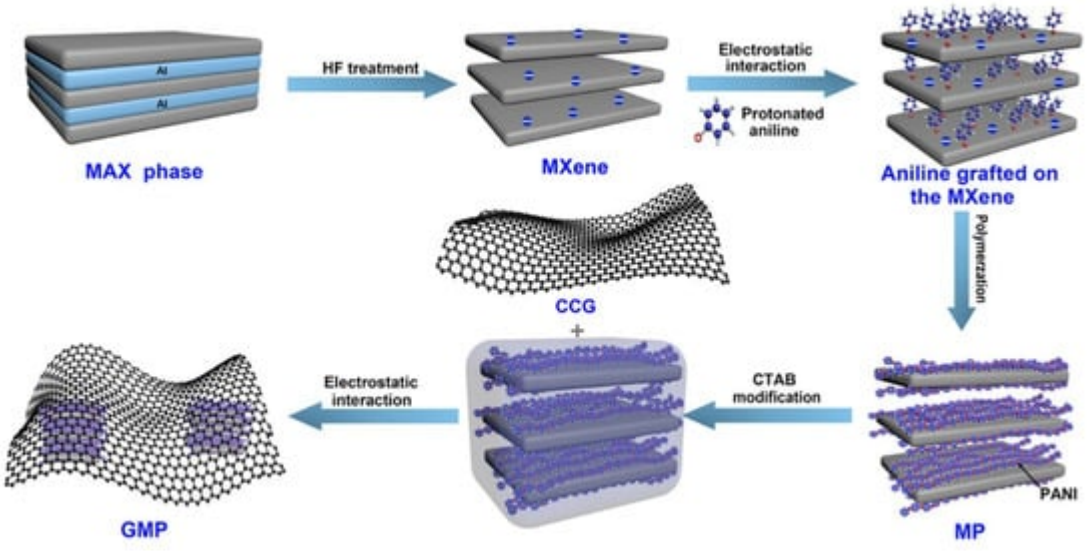

Figure 4. Scheme of the synthesis of graphene-encapsulated Ti_2CT_x@PANI hybrid (GMP); Reproduced with permission [42]. Copyright 2018, American Chemical Society.

When turning to the other common-used conducting polymer, poly(3,4-ethylene dioxythiophene) (PEDOT), Gogotsi and his co-workers revealed the mechanism of charge-transfer-induced polymerization of EDOT on the surface of $Ti_3C_2T_x$ MXene [44]. Verified by the theoretical calculations, the parallel orientation of EDOT monomer on $Ti_3C_2T_x$ surface presented the most stable configuration with the lowest binding energy of −1.02 eV. After adsorption, 0.34 electrons were transferred from EDOT to $Ti_3C_2O_2$, which initiated the in situ polymerization of EDOT on $Ti_3C_2O_2$. With the energy supplement via electrochemical reaction, Qin et al. demonstrated a one-step in situ electrochemical polymerization for $Mo_{1.33}C$/PEDOT and $Ti_3C_2T_x$/PEDOT films with controlled thickness and micropattern [45]. However, due to the insoluble nature of PEDOT, the commercial product usually contains a mixture of poly(styrene sulfonate) (PSS). In consideration of the bicomponent structure and the ionic chain nature, the ex-suit blending method was more popular than in-suit polymerization towards MXene-PEDOT:PSS hybrids and the electrostatic interaction between PSS and MXene promoted the formation of 3D interconnected and reticulated structure. The hydrogen from $–SO_3H$ on PEDOT:PSS with –OH,–F on $Ti_3C_2T_x$ and the electrostatic interaction between PSS and MXene were also found to jointly shield the coulombic attraction between PEDOT and PSS, which enhanced the inter-chain charge transport between PEDOT chains [46]. The $Ti_3C_2T_x$/(PEDOT:PSS) film can be fabricated by drop-casting [47], vacuum-assisted filtration [48], and simply filtration [49][50]. Recently, MXene/(PEDOT:PSS) hybrid was also fabricated into a fiber-shaped supercapacitor by a one-step wet-spinning approach [51].

By the ex-situ blending method, plenty of MXene/polymers hydrides can be prepared. Firstly reported by Gogotsi et al., charged poly-diallyl dimethyl ammonium chloride (PDDA) and electrically neutral polyvinyl alcohol (PVA) were blended with $Ti_3C_2T_x$ by vacuum-assisted filtration [52]. Subsequently, the dispersibility of MXene sheets in the PVA matrix and the dielectric performance of MXene/PVA hybrids in X-band frequency was studied [53]. Boota et al. synthesized polyfluorene (PFO) derivatives containing nonpolar, polar nitrogen-containing, and charged nitrogen-containing lateral chains by Suzuki polycondensation reaction (Figure 3b) [36]. They have pointed out that both the electrostatic interactions and hydrogen bonds may be involved between MXene and PFO derivatives. However, the bulky methyl groups from polar polymers with charged nitrogen-containing ends prohibited the formation of the hydrogen bond. A physical vapor deposition technique, resonant infrared matrix-assisted pulsed laser evaporation (RIR-MAPLE), was performed by Ajnsztajn et al. to produce $Ti_3C_2T_x$/PFO transparent hybrid electrode [54]. Via RIR-MAPLE, the film exhibited the minimal phase segregation.

4. MXene-Organic Hybrids through Hydrogen Bonds and Other Supermolecular Interactions

Except for the strong inorganic-organic correlation provided by covalent and electrostatic interaction, the supermolecular interactions are also critical to the formation of MXene-organic hybrids. In 2016, a $Ti_3C_2T_x$/polypyrrole (PPy) hybrid with highly aligned PPy chains in between the $Ti_3C_2T_x$ layers was prepared by unconventional oxidant-free polymerization (Figure 5a) [55]. Specifically, the key factor in the alignment process was the hydrogen bond, which might originate from the N–H group of the pyrrole ring and terminating oxygen or fluorine on the $Ti_3C_2T_x$ surface. What is more, the fluorine on $Ti_3C_2T_x$ will be doped in PPy chains, which can further enhance their electrochemical activity. Different from the oxidant-free chemical polymerization, Zhu et al. [56] fabricated $Ti_3C_2T_x$/PPy hybrid film via electrophoretic deposition and electrochemical polymerization. The pronounced acidic character of the $Ti_3C_2T_x$ surface generated hydrogen bonding between $Ti_3C_2T_x$ and PPy during electrochemical polymerization. However, for the most traditional pyrrole polymerization [57], $FeCl_3{\cdot}6H_2O$ was applied as an oxidant, and the strong oxidizing Fe^{3+} ions will result in the oxidation of $Ti_3C_2T_x$. Therefore, Zhang et al. only found the 3D TiO_2@NC/Fe_7S_8 hybrids by in situ polymerization of pyrrole monomer with alkalized $Ti_3C_2T_x$.

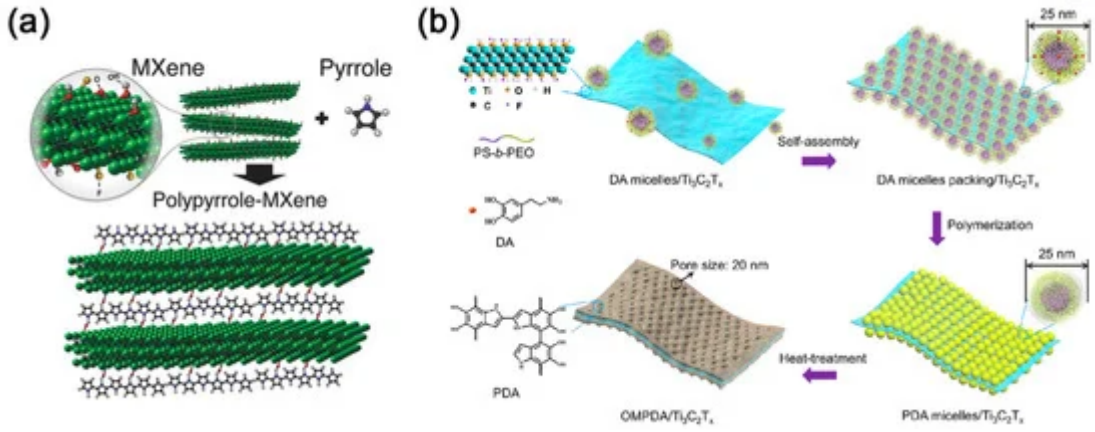

Figure 5. (**a**) Schematic illustration of pyrrole polymerization using MXene; reproduced with permission [55]. Copyright 2016, WILEY-VCH. (**b**) Schematic drawing depicting the preparation steps of OMPDA/$Ti_3C_2T_x$ hybrid: (i)

mixing the DAmi with $Ti_3C_2T_x$ nanosheets, (ii) packing of DAmi and subsequent, (iii) direct polymerization of polydopamine (PDA) micelles on the surface of $Ti_3C_2T_x$ nanosheets, and (iv) obtaining the OMPDA/$Ti_3C_2T_x$ after heat treatment; Reproduced with permission [58]. Copyright 2020, American Chemical Society.

As confirmed by previous studies, quinones are important redox-active centers for the chemical reaction [59]. However, there are only a limited amount of quinones reserved in polydopamine (PDA), which is positively correlated to the oxidation state of PDA [60]. Interestingly, $Ti_3C_2T_x$/PDA hybrids were found to be an excellent precursor for o-benzoquinone after low-temperature heat treatment at 300 °C [59]. After that, Li et al. further prepared vertically oriented ordered mesopores (OM) PDA/$Ti_3C_2T_x$ hybrid (OMPDA/$Ti_3C_2T_x$) by using the PS-b-PEO block polymer as a soft-template (Figure 5b) [58]. In their report, the hydrogen bond also played a crucial role in the assembly of dopamine/PS-b-PEO micelles and $Ti_3C_2T_x$. Recently, Du and coworkers utilized $Ti_3C_2T_x$@PDA prepared by in situ polymerization as starting materials to hybrid with poly(ethylene glycol) (PEG)-based polyurethane (PU) [61]. The PDA is found to be a medium molecule that facilitated the interfacial compatibility of $Ti_3C_2T_x$ flakes in PEG-based PU, where the $Ti_3C_2T_x$@PDA covalently bonded with PU during the process of copolymerization.

Beyond anchoring the organic species on the MXene surface, the hydrogen bond also functions as a flexible junction between the inorganic MXene and organic part. Hybrid consisting of $Ti_3C_2T_x$ and polyacrylamide (PAM) was fabricated by Niu et al. [29]. In 2020, the exfoliated $Ti_3C_2T_x$ nanosheets were reported for the first time that acted as a crosslinker instead of traditional organic molecules. In the hybrid, hydrogen bonding between the –$CONH_2$ groups from PAM chains and the hydrophilic groups (–OH and –F) from the $Ti_3C_2T_x$ nanosheets were observed. Zhang et al. simply prepared MXene hydrogel hybrids by mixing $Ti_3C_2T_x$ MXene and commercial polyvinyl alcohol (PVA) hydrogel [62]. They indicated the secondary crosslinking between MXene and PVA and a dense network yielded by polymer chain entanglements. Xuan et al. improved this method by added MXene flakes into a homogeneous PVA solution [63], with the borate solution acting as the crosslinking agent, MXene bonding with PVA chains, and tetra-functional borate ion covalently. A similar interaction was also found in hydrophobically associated dry polyacrylamide (HAPAM) hydrogel [64]. In HAPAM hydrogel, hydrogen bonds between MXene and amide group of HAPAM became additional crosslinking points, which contributed to the hybrid double-network with N,N'-methylene diacryl amide (MBAA) crosslinker and affected the self-healing ability and temperature sensibility. When there were two or more different kinds of monomers or polymers together with MXene nanosheets, MXene-copolymeric hydrogels can also be prepared [65][66][67].

On the aspect of ex situ blending, Le et al. intertwined $Ti_3C_2T_x$ MXene particles in tangled PPy nanowires through hydrogen bond [68]. The intercalated PPy chains between the conductive $Ti_3C_2T_x$ sheets prevented the dense stacking of $Ti_3C_2T_x$. Meanwhile, the intercalation further improved the structural stability of PPy backbones. Moreover, $Ti_3C_2T_x$ MXene and PANI hybrid was also prepared by mechanical blending [69]. The lightweight $Ti_3C_2T_x$/PANI hybrids for EMI shielding was obtained by simply mixing PANI powder with MXene powder. The authors suggested that an equal concentration of both materials would be beneficial for enhanced interfacial interaction between them.

Except for hydrogen, the polymer chain entanglements, ionic interactions, covalent bonding were also reported, and the role of MXene sheets in hydrogel varies [65]. MXene polymer hydrogel was gradually developed with improved performance. The typical interactions between MXene and organic modified species are summarized in Table 1.

Table 1. Summary of the interactions between MXene and organic species.

Interaction Type	Typical Modifier	Binding Forms
Covalent interaction	Silane	[a] Si–O–M
	Diazonium salts	C–O–M
	Alkyl phosphoric acid	P–O–M
Electrostatic interaction	Alkyl ammonium salts	[b] $R_4N^{\oplus}$ $^{\ominus}$T–M
	Amino acids	$–H_3N^{\oplus}$ $^{\ominus}$T–M
	PFO	$R_4N^{\oplus}$ $^{\ominus}$T–M
	PANI	$–H_3N^{\oplus}$ $^{\ominus}$T–M
	PEDOT:PSS	$SO_3H^{\oplus}$ $^{\ominus}$T–M
Hydrogen bonds	Pyrrole/PPy	NH···O–M
	Dopamine/PDA	OH···O–M
	PAM	$CONH_2$···O–M
	PVA	OH···O–M
	PSS	SO_3H···O–M

[a] M represents a metal atom from the surface layer of MXenes. [b] R represents any alkyl group.

References

1. Naguib, M.; Kurtoglu, M.; Presser, V.; Lu, J.; Niu, J.J.; Heon, M.; Hultman, L.; Gogotsi, Y.; Barsoum, M.W. Two-Dimensional Nanocrystals Produced by Exfoliation of Ti3AlC2. Adv. Mater. 2011, 23, 4248–4253, doi:10.1002/adma.201102306.
2. Yu, H.; Wang, Y.; Jing, Y.; Ma, J.; Du, C.F.; Yan, Q. Surface modified MXene-based nanocomposites for electrochemical energy conversion and storage. Small 2019, 15, 1901503, doi:10.1002/smll.201901503.

3. Zhang, C.J.; Pinilla, S.; McEvoy, N.; Cullen, C.P.; Anasori, B.; Long, E.; Park, S.-H.; Seral-Ascaso, A.; Shmeliov, A.; Krishnan, D.; et al. Oxidation Stability of Colloidal Two-Dimensional Titanium Carbides (MXenes). Chem. Mater. 2017, 29, 4848–4856, doi:10.1021/acs.chemmater.7b00745.
4. Rozmyslowska, A.; Wojciechowski, T.; Ziemkowska, W.; Chlubny, L.; Olszyna, A.; Pozniak, S.; Tomkiewicz, K.; Jastrzebska, A.M. Colloidal Properties and Stability of 2D Ti3C2 and Ti2C MXenes in Water. Int. J. Electrochem. Sci. 2018, 13, 10837–10847, doi:10.20964/2018.11.56.
5. Maleski, K.; Mochalin, V.N.; Gogotsi, Y. Dispersions of Two-Dimensional Titanium Carbide MXene in Organic Solvents. Chem. Mater. 2017, 29, 1632–1640, doi:10.1021/acs.chemmater.6b04830.
6. Carey, M.; Hinton, Z.; Natu, V.; Pai, R.; Sokol, M.; Alvarez, N.J.; Kalra, V.; Barsoum, M.W. Dispersion and Stabilization of Alkylated 2D MXene in Nonpolar Solvents and Their Pseudocapacitive Behavior. Cell Rep. Phys. Sci. 2020, 1, 100042, doi:10.1016/j.xcrp.2020.100042.
7. Du, Y.; Yu, B.; Wei, L.; Wang, Y.; Zhang, X.; Ye, S. Efficient removal of Pb(II) by Ti3C2Tx powder modified with a silane coupling agent. J. Mater. Sci. 2019, 54, 13283–13297, doi:10.1007/s10853-019-03814-z.
8. Zhao, J.; Yang, Y.; Yang, C.; Tian, Y.; Han, Y.; Liu, J.; Yin, X.; Que, W. A hydrophobic surface enabled salt-blocking 2D Ti3C2 MXene membrane for efficient and stable solar desalination. J. Mater. Chem. A 2018, 6, 16196–16204, doi:10.1039/c8ta05569f.
9. Lim, S.; Park, H.; Yang, J.; Kwak, C.; Lee, J. Stable colloidal dispersion of octylated Ti3C2-MXenes in a nonpolar solvent. Colloid Surf. A-Phys. . Eng. Asp. 2019, 579, 123648, doi:10.1016/j.colsurfa.2019.123648.
10. Zhang, Q.; Yi, G.; Fu, Z.; Yu, H.; Chen, S.; Quan, X. Vertically Aligned Janus MXene-Based Aerogels for Solar Desalination with High Efficiency and Salt Resistance. ACS Nano 2019, 13, 13196–13207, doi:10.1021/acsnano.9b06180.
11. Tran, M.H.; Brilmayer, R.; Liu, L.; Zhuang, H.; Hess, C.; Andrieu-Brunsen, A.; Birkel, C.S. Synthesis of a Smart Hybrid MXene with Switchable Conductivity for Temperature Sensing. ACS Appl. Nano Mater. 2020, 3, 4069–4076, doi:10.1021/acsanm.0c00118.
12. Taloub, N.; Henniche, A.; Liu, L.; Li, J.; Rahoui, N.; Hegazy, M.; Huang, Y.D. Improving the mechanical properties, UV and hydrothermal aging resistance of PIPD fiber using MXene (Ti3C2(OH)2) nanosheets. Compos. Part B-Eng. 2019, 163, 260–271, doi:10.1016/j.compositesb.2018.11.007.
13. Riazi, H.; Anayee, M.; Hantanasirisakul, K.; Shamsabadi, A.A.; Anasori, B.; Gogotsi, Y.; Soroush, M. Surface Modification of a MXene by an Aminosilane Coupling Agent. Adv. Mater. Interfaces 2020, 7, 1902008, doi:10.1002/admi.201902008.

14. Kim, D.; Ko, T.Y.; Kim, H.; Lee, G.H.; Cho, S.; Koo, C.M. Nonpolar Organic Dispersion of 2D Ti3C2Tx MXene Flakes via Simultaneous Interfacial Chemical Grafting and Phase Transfer Method. ACS Nano 2019, 13, 13818–13828, doi:10.1021/acsnano.9b04088.
15. Sun, W.J.; Zhao, Y.Y.; Cheng, X.F.; He, J.H.; Lu, J.M. Surface Functionalization of Single-Layered Ti3C2Tx MXene and Its Application in Multilevel Resistive Memory. ACS Appl. Mater. Interfaces 2020, 12, 9865–9871, doi:10.1021/acsami.9b16979.
16. Zhang, P.; Wang, L.; Huang, Z.; Yu, J.; Li, Z.; Deng, H.; Yin, T.; Yuan, L.; Gibson, J.K.; Mei, L.; et al. Aryl Diazonium-Assisted Amidoximation of MXene for Boosting Water Stability and Uranyl Sequestration via Electrochemical Sorption. ACS Appl. Mater. Interfaces 2020, 12, 15579–15587, doi:10.1021/acsami.0c00861.
17. Zhang, P.; Wang, L.; Du, K.; Wang, S.; Huang, Z.; Yuan, L.; Li, Z.; Wang, H.; Zheng, L.; Chai, Z.; et al. Effective removal of U(VI) and Eu(III) by carboxyl functionalized MXene nanosheets. J. Hazard. Mater. 2020, 396, 122731, doi:10.1016/j.jhazmat.2020.122731.
18. Wang, H.; Zhang, J.; Wu, Y.; Huang, H.; Li, G.; Zhang, X.; Wang, Z. Surface modified MXene Ti3C2 multilayers by aryl diazonium salts leading to large-scale delamination. Appl. Surf. Sci. 2016, 384, 287–293, doi:10.1016/j.apsusc.2016.05.060.
19. Wang, H.; Zhang, J.; Wu, Y.; Huang, H.; Jiang, Q. Chemically functionalized two-dimensional titanium carbide MXene by in situ grafting-intercalating with diazonium ions to enhance supercapacitive performance. J. Phys. Chem. Solids 2018, 115, 172–179, doi:10.1016/j.jpcs.2017.12.039.
20. Chen, K.; Yan, X.; Li, J.; Jiao, T.; Cai, C.; Zou, G.; Wang, R.; Wang, M.; Zhang, L.; Peng, Q. Preparation of Self-Assembled Composite Films Constructed by Chemically-Modified MXene and Dyes with Surface-Enhanced Raman Scattering Characterization. Nanomaterials 2019, 9, 284, doi:10.3390/nano9020284.
21. Boota, M.; Urbankowski, P.; Porzio, W.; Barba, L.; Osti, N.C.; Bleuel, M.; Keum, J.K.; Mamontov, E. Understanding Functionalization of Titanium Carbide (MXene) with Quinones and Their Pseudocapacitance. ACS Appl. Energy Mater. 2020, 3, 4127–4133, doi:10.1021/acsaem.0c00314.
22. Zhang, H.; Wang, L.B.; Chen, Q.; Li, P.; Zhou, A.G.; Cao, X.X.; Hu, Q.K. Preparation, mechanical and anti-friction performance of MXene/polymer composites. Mater. Des. 2016, 92, 682–689, doi:10.1016/j.matdes.2015.12.084.
23. Sliozberg, Y.; Andzelm, J.; Hatter, C.B.; Anasori, B.; Gogotsi, Y.; Hall, A. Interface binding and mechanical properties of MXene-epoxy nanocomposites. Compos. Sci. Technol. 2020, 192, 108124, doi:10.1016/j.compscitech.2020.108124.

24. Zhi, W.; Xiang, S.; Bian, R.; Lin, R.; Wu, K.; Wang, T.; Cai, D. Study of MXene-filled polyurethane nanocomposites prepared via an emulsion method. Compos. Sci. Technol. 2018, 168, 404–411, doi:10.1016/j.compscitech.2018.10.026.

25. Malaki, M.; Varma, R.S. Mechanotribological Aspects of MXene-Reinforced Nanocomposites. Adv. Mater. 2020, 32, 2003154, doi:10.1002/adma.202003154.

26. Hai, Y.; Jiang, S.; Zhou, C.; Sun, P.; Huang, Y.; Niu, S. Fire-safe unsaturated polyester resin nanocomposites based on MAX and MXene: A comparative investigation of their properties and mechanism of fire retardancy. Dalton Trans. 2020, 49, 5803–5814, doi:10.1039/d0dt00686f.

27. He, L.; Wang, J.; Wang, B.; Wang, X.; Zhou, X.; Cai, W.; Mu, X.; Hou, Y.; Hu, Y.; Song, L. Large-scale production of simultaneously exfoliated and Functionalized Mxenes as promising flame retardant for polyurethane. Compos. Part B-Eng. 2019, 179, 107486, doi:10.1016/j.compositesb.2019.107486.

28. Chen, J.; Chen, K.; Tong, D.; Huang, Y.; Zhang, J.; Xue, J.; Huang, Q.; Chen, T. CO2 and temperature dual responsive "Smart" MXene phases. Chem. Commun. 2015, 51, 314–317, doi:10.1039/c4cc07220k.

29. Zhang, P.; Yang, X.-J.; Li, P.; Zhao, Y.; Niu, Q.J. Fabrication of novel MXene (Ti3C2)/polyacrylamide nanocomposite hydrogels with enhanced mechanical and drug release properties. Soft Matter 2020, 16, 162–169, doi:10.1039/c9sm01985e.

30. Cui, Y.; Wang, J.; Wang, X.; Qin, J.; Cao, M. A Hybrid Assembly of MXene with NH2−Si Nanoparticles Boosting Lithium Storage Performance. Chem. Asian J. 2020, 15, 1376–1383, doi:10.1002/asia.202000017.

31. Xu, B.; Zhu, M.; Zhang, W.; Zhen, X.; Pei, Z.; Xue, Q.; Zhi, C.; Shi, P. Ultrathin MXene-Micropattern-Based Field-Effect Transistor for Probing Neural Activity. Adv. Mater. 2016, 28, 3333–3339, doi:10.1002/adma.201504657.

32. Luo, J.; Zheng, J.; Nai, J.; Jin, C.; Yuan, H.; Sheng, O.; Liu, Y.; Fang, R.; Zhang, W.; Huang, H.; et al. Atomic Sulfur Covalently Engineered Interlayers of Ti3C2 MXene for Ultra-Fast Sodium-Ion Storage by Enhanced Pseudocapacitance. Adv. Funct. Mater. 2019, 29, 1808107, doi:10.1002/adfm.201808107.

33. Luo, J.; Zhang, W.; Yuan, H.; Jin, C.; Zhang, L.; Huang, H.; Liang, C.; Xia, Y.; Zhang, J.; Gan, Y.; et al. Pillared Structure Design of MXene with Ultralarge Interlayer Spacing for High-Performance Lithium-Ion Capacitors. ACS Nano 2017, 11, 2459–2469, doi:10.1021/acsnano.6b07668.

34. Si, J.Y.; Tawiah, B.; Sun, W.L.; Lin, B.; Wang, C.; Yuen, A.C.Y.; Yu, B.; Li, A.; Yang, W.; Lu, H.D.; et al. Functionalization of MXene Nanosheets for Polystyrene towards High Thermal Stability and Flame Retardant Properties. Polymers 2019, 11, 976, doi:10.3390/polym11060976.

35. Bian, R.; Lin, R.; Wang, G.; Lu, G.; Zhi, W.; Xiang, S.; Wang, T.; Clegg, P.S.; Cai, D.; Huang, W. 3D assembly of Ti3C2-MXene directed by water/oil interfaces. Nanoscale 2018, 10, 3621–3625, doi:10.1039/c7nr07346a.

36. Boota, M.; Pasini, M.; Galeotti, F.; Porzio, W.; Zhao, M.-Q.; Halim, J.; Gogotsi, Y. Interaction of Polar and Nonpolar Polyfluorenes with Layers of Two-Dimensional Titanium Carbide (MXene): Intercalation and Pseudocapacitance. Chem. Mater. 2017, 29, 2731–2738, doi:10.1021/acs.chemmater.6b03933.

37. Elumalai, S.; Yoshimura, M.; Ogawa, M. Simultaneous Delamination and Rutile Formation on the Surface of Ti3C2Tx MXene for Copper Adsorption. Chem. Asian J. 2020, 15, 1044–1051, doi:10.1002/asia.202000090.

38. Chen, C.; Boota, M.; Urbankowski, P.; Anasori, B.; Miao, L.; Jiang, J.J.; Gogotsi, Y. Effect of glycine functionalization of 2D titanium carbide (MXene) on charge storage. J. Mater. Chem. A 2018, 6, 4617–4622, doi:10.1039/c7ta11347a.

39. Carey, M.; Hinton, Z.; Sokol, M.; Alvarez, N.J.; Barsoum, M.W. Nylon-6/Ti3C2Tz MXene Nanocomposites Synthesized by in Situ Ring Opening Polymerization of epsilon-Caprolactam and Their Water Transport Properties. ACS Appl. Mater. Interfaces 2019, 11, 20425–20436, doi:10.1021/acsami.9b05027.

40. Carey, M.S.; Sokol, M.; Palmese, G.R.; Barsoum, M.W. Water Transport and Thermomechanical Properties of Ti3C2Tz MXene Epoxy Nanocomposites. ACS Appl. Mater. Interfaces 2019, 11, 39143–39149, doi:10.1021/acsami.9b11448.

41. Wang, Y.; Gao, X.; Zhang, L.J.; Wu, X.M.; Wang, Q.G.; Luo, C.Y.; Wu, G.L. Synthesis of Ti3C2/Fe3O4/PANI hierarchical architecture composite as an efficient wide-band electromagnetic absorber. Appl. Surf. Sci. 2019, 480, 830–838, doi:10.1016/j.apsusc.2019.03.049.

42. Fu, J.; Yun, J.; Wu, S.; Li, L.; Yu, L.; Kim, K.H. Architecturally Robust Graphene-Encapsulated MXene Ti2CTx@Polyaniline Composite for High-Performance Pouch-Type Asymmetric Supercapacitor. ACS Appl. Mater. Interfaces 2018, 10, 34212–34221, doi:10.1021/acsami.8b10195.

43. Xu, H.; Zheng, D.; Liu, F.; Li, W.; Lin, J. Synthesis of an MXene/polyaniline composite with excellent electrochemical properties. J. Mater. Chem. A 2020, 8, 5853–5858, doi:10.1039/d0ta00572j.

44. Chen, C.; Boota, M.; Xie, X.; Zhao, M.; Anasori, B.; Ren, C.E.; Miao, L.; Jiang, J.; Gogotsi, Y. Charge transfer induced polymerization of EDOT confined between 2D titanium carbide layers. J. Mater. Chem. A 2017, 5, 5260–5265, doi:10.1039/C7TA00149E.

45. Qin, L.; Tao, Q.; Liu, X.; Fahlman, M.; Halim, J.; Perssona, P.O.A.; Rosen, J.; Zhang, F. Polymer-MXene composite films formed by MXene-facilitated electrochemical polymerization for flexible

solid-state microsupercapacitors. Nano Energy 2019, 60, 734–742, doi:10.1016/j.nanoen.2019.04.002.

46. Hou, C.; Yu, H. Modifying the nanostructures of PEDOT:PSS/Ti3C2TX composite hole transport layers for highly efficient polymer solar cells. J. Mater. Chem. C 2020, 8, 4169–4180, doi:10.1039/d0tc00075b.
47. Wang, X.; Sun, K.; Li, K.; Li, X.; Gogotsi, Y. Ti3C2Tx/PEDOT:PSS hybrid materials for room-temperature methanol sensor. Chin. Chem. Lett. 2020, 31, 1018–1021, doi:10.1016/j.cclet.2019.11.031.
48. Liu, R.; Miao, M.; Li, Y.; Zhang, J.; Cao, S.; Feng, X. Ultrathin Biomimetic Polymeric Ti3C2Tx MXene Composite Films for Electromagnetic Interference Shielding. ACS Appl. Mater. Interfaces 2018, 10, 44787–44795, doi:10.1021/acsami.8b18347.
49. Qin, L.; Tao, Q.; El Ghazaly, A.; Fernandez-Rodriguez, J.; Persson, P.O.Å.; Rosen, J.; Zhang, F. High-Performance Ultrathin Flexible Solid-State Supercapacitors Based on Solution Processable Mo1.33C MXene and PEDOT:PSS. Adv. Funct. Mater. 2018, 28, doi:10.1002/adfm.201703808.
50. Li, L.; Zhang, N.; Zhang, M.; Zhang, X.; Zhang, Z. Flexible Ti3C2Tx/PEDOT:PSS films with outstanding volumetric capacitance for asymmetric supercapacitors. Dalton Trans. 2019, 48, 1747–1756, doi:10.1039/c8dt04374d.
51. Zhang, J.; Seyedin, S.; Qin, S.; Wang, Z.; Moradi, S.; Yang, F.; Lynch, P.A.; Yang, W.; Liu, J.; Wang, X.; et al. Highly Conductive Ti3C2Tx MXene Hybrid Fibers for Flexible and Elastic Fiber-Shaped Supercapacitors. Small 2019, 15, 1804732, doi:10.1002/smll.201804732.
52. Ling, Z.; Ren, C.E.; Zhao, M.Q.; Yang, J.; Giammarco, J.M.; Qiu, J.S.; Barsoum, M.W.; Gogotsi, Y. Flexible and conductive MXene films and nanocomposites with high capacitance. Proc. Natl. Acad. Sci. USA 2014, 111, 16676–16681, doi:10.1073/pnas.1414215111.
53. Mirkhani, S.A.; Zeraati, A.S.; Aliabadian, E.; Naguib, M.; Sundararaj, U. High Dielectric Constant and Low Dielectric Loss via Poly(vinyl alcohol)/Ti3C2Tx MXene Nanocomposites. ACS Appl. Mater. Interfaces 2019, 11, 18599–18608, doi:10.1021/acsami.9b00393.
54. Ajnsztajn, A.; Ferguson, S.; Thostenson, J.O.; Ngaboyamahina, E.; Parker, C.B.; Glass, J.T.; Stiff-Roberts, A.D. Transparent MXene-Polymer Supercapacitive Film Deposited Using RIR-MAPLE. Crystals 2020, 10, 152, doi:10.3390/Cryst10030152.
55. Boota, M.; Anasori, B.; Voigt, C.; Zhao, M.Q.; Barsoum, M.W.; Gogotsi, Y. Pseudocapacitive Electrodes Produced by Oxidant-Free Polymerization of Pyrrole between the Layers of 2D Titanium Carbide (MXene). Adv. Mater. 2016, 28, 1517–1522, doi:10.1002/adma.201504705.
56. Zhu, M.; Huang, Y.; Deng, Q.; Zhou, J.; Pei, Z.; Xue, Q.; Huang, Y.; Wang, Z.; Li, H.; Huang, Q.; et al. Highly Flexible, Freestanding Supercapacitor Electrode with Enhanced Performance Obtained

by Hybridizing Polypyrrole Chains with MXene. Adv. Energy Mater. 2016, 6, 1600969, doi:10.1002/aenm.201600969.

57. Zhang, X.; Li, J.; Li, J.; Han, L.; Lu, T.; Zhang, X.; Zhu, G.; Pan, L. 3D TiO2@nitrogen-doped carbon/Fe7S8 composite derived from polypyrrole-encapsulated alkalized MXene as anode material for high-performance lithium-ion batteries. Chem. Eng. J. 2020, 385, 123394, doi:10.1016/j.cej.2019.123394.
58. Li, T.; Ding, B.; Wang, J.; Qin, Z.; Fernando, J.F.S.; Bando, Y.; Nanjundan, A.K.; Kaneti, Y.V.; Golberg, D.; Yamauchi, Y. Sandwich-Structured Ordered Mesoporous Polydopamine/MXene Hybrids as High-Performance Anodes for Lithium-Ion Batteries. ACS Appl. Mater. Interfaces 2020, 12, 14993–15001, doi:10.1021/acsami.9b18883.
59. Dong, X.; Ding, B.; Guo, H.; Dou, H.; Zhang, X. Superlithiated Polydopamine Derivative for High-Capacity and High-Rate Anode for Lithium-Ion Batteries. ACS Appl. Mater. Interfaces 2018, 10, 38101–38108, doi:10.1021/acsami.8b13998.
60. Sun, T.; Li, Z.J.; Wang, H.G.; Bao, D.; Meng, F.L.; Zhang, X.B. A Biodegradable Polydopamine-Derived Electrode Material for High-Capacity and Long-Life Lithium-Ion and Sodium-Ion Batteries. Angew. Chem. Int. Ed. Engl. 2016, 55, 10662–10666, doi:10.1002/anie.201604519.
61. Du, X.; Qiu, J.; Deng, S.; Du, Z.; Cheng, X.; Wang, H. Ti3C2Tx@PDA-Integrated Polyurethane Phase Change Composites with Superior Solar-Thermal Conversion Efficiency and Improved Thermal Conductivity. ACS Sustain. Chem. Eng. 2020, 8, 5799–5806, doi:10.1021/acssuschemeng.0c01582.
62. Zhang, Y.Z.; Lee, K.H.; Anjum, D.H.; Sougrat, R.; Jiang, Q.; Kim, H.; Alshareef, H.N. MXenes stretch hydrogel sensor performance to new limits. Sci. Adv. 2018, 4, eaat0098, doi:10.1126/sciadv.aat0098.
63. Zhang, J.; Wan, L.; Gao, Y.; Fang, X.; Lu, T.; Pan, L.; Xuan, F. Highly Stretchable and Self-Healable MXene/Polyvinyl Alcohol Hydrogel Electrode for Wearable Capacitive Electronic Skin. Adv. Electron. Mater. 2019, 5, 1900285, doi:10.1002/aelm.201900285.
64. Zhang, Y.; Chen, K.; Li, Y.; Lan, J.; Yan, B.; Shi, L.; Ran, R. High-Strength, Self-Healable, Temperature-Sensitive, MXene-Containing Composite Hydrogel as a Smart Compression Sensor. ACS Appl. Mater. Interfaces 2019, 11, 47350–47357, doi:10.1021/acsami.9b16078.
65. Zhang, Y.Z.; El-Demellawi, J.K.; Jiang, Q.; Ge, G.; Liang, H.; Lee, K.; Dong, X.; Alshareef, H.N. MXene hydrogels: Fundamentals and applications. Chem. Soc. Rev. 2020, 49, 7229–7251, doi:10.1039/d0cs00022a.
66. Liao, H.; Guo, X.; Wan, P.; Yu, G. Conductive MXene Nanocomposite Organohydrogel for Flexible, Healable, Low-Temperature Tolerant Strain Sensors. Adv. Funct. Mater. 2019, 29, 1904507, doi:10.1002/adfm.201904507.

67. Wu, X.; Liao, H.; Ma, D.; Chao, M.; Wang, Y.; Jia, X.; Wan, P.; Zhang, L. A wearable, self-adhesive, long-lastingly moist and healable epidermal sensor assembled from conductive MXene nanocomposites. J. Mater. Chem. C 2020, 8, 1788–1795, doi:10.1039/c9tc05575d.
68. Le, T.A.; Tran, N.Q.; Hong, Y.; Lee, H. Intertwined Titanium Carbide MXene within a 3 D Tangled Polypyrrole Nanowires Matrix for Enhanced Supercapacitor Performances. Chem. Eur. J. 2019, 25, 1037–1043, doi:10.1002/chem.201804291.
69. Kumar, S.; Arti; Kumar, P.; Singh, N.; Verma, V. Steady microwave absorption behavior of two-dimensional metal carbide MXene and Polyaniline composite in X-band. J. Magn. Magn. Mater. 2019, 488, 165364, doi:10.1016/J.Jmmm.2019.165364.